ELSEVIER

Mathematical Biosciences 156 (1999) 207–228

Mathematical Biosciences
an international journal

Cytoplasm dynamics and cell motion: two-phase flow models

Wolfgang Alt [a,*], Micah Dembo [b]

[a] *Theoretical Biology, University of Bonn, Kirschallee 1, D-53115 Bonn, Germany*
[b] *Biomedical Engineering, Boston University, 44 Cummington Street, MA 02215-2407, USA*

Received 26 February 1998; accepted 12 July 1998

Abstract

The motion of amoeboid cells is characterized by cytoplasmic streaming and by membrane protrusions and retractions which occur even in the absence of interactions with a substratum. Cell translocation requires, in addition, a transmission mechanism wherein the power produced by the cytoplasmic engine is applied to the substratum in a highly controlled fashion through specific adhesion proteins. Here we present a simple mechano-chemical model that tries to capture the physical essence of these complex biomolecular processes. Our model is based on the continuum equations for a viscous and reactive two-phase fluid model with moving boundaries, and on force balance equations that average the stochastic interactions between actin polymers and membrane proteins. In this paper we present a new derivation and analysis of these equations based on minimization of a power functional. This derivation also leads to a clear formulation and classification of the kinds of boundary conditions that should be specified at free surfaces and at the sites of interaction of the cell and the substratum. Numerical simulations of a one-dimensional lamella reveal that even this extremely simplified model is capable of producing several typical features of cell motility. These include periodic 'ruffle' formation, protrusion–retraction cycles, centripetal flow and cell-substratum traction forces.

Keywords: Cytoplasm dynamics; Cell motion; Two-phase flow; Reactive fluids; Hyperbolic–elliptic system; Free boundary value problem

* Corresponding author. Tel.: +49-228 735 577; fax: +49-228 735 5513; e-mail: wolf.alt@uni-bonn.de

0025-5564/99/$ – see front matter
PII: S0025-5564(98)10067-6

1. Cell division and cell locomotion: modelling of cytoplasmic interactions

For most biological cells functionality and survival ultimately depend on motion. This requirement is quite obvious in the case of cell division and cell locomotion. In the case of division, during the later stages of *cytokinesis*, eukaryotic cells have to divide into two halves precisely at the 'equatorial plane', where cleavage furrows are intensified and successively deepened to form the constriction ring, which finally splits the cell. Responsible for this accurate dynamical event are *actin filaments* which preferably assemble near the cell cortex and induce there a quasi-steady cortical flow in the region of the furrow (see Fig. 1 in Ref. [7]).

The molecular systems that produce these motions have been highly conserved in evolution and for the most part are close relatives of the proteins that constitute the sarcomeres of muscle cells. In particular, in both muscle cells and amoeboid cells, polymeric actin is present in abundance and forms a meshwork of overlapping filaments in the cytoplasm. In both cell types the actin filaments are linked to membrane structures and are cross-linked to each other by homologous actin binding proteins. Finally, polymers of *myosin* are interspersed among the actin filaments. These molecular motor proteins exert contractile forces on the actin network and they provide the major source of mechanical power in muscle cells. It is clear that the myosin molecules also function to produce mechanical power for motility in the non-muscle cells, however, one cannot discount the possibility that these cells also employ additional mechanisms (see further discussion below).

Typical motions of non-muscle cells are much slower than muscle twitches and the rates for polymerization and depolymerization of the cytoskeleton are much faster. As a result the time scale for a complete chemical cycle of formation and breakdown of the cytoskeleton in a typical amoeboid cell is similar to, or even faster than, the functional time scale. Thus, for example, it has been estimated that the cytoskeleton of a crawling cell can undergo several complete chemical cycles during the time it takes to move one cell diameter [26]. Moreover, the transient nature of the linkages that interconnect the various components of the amoeboid cytoskeleton imply that the overall structure is programmed to easily relax and adapt itself completely even in the face of very large deformations. This conclusion is consistent with those few cases where detailed studies of the passive deformation of amoeboid cells have been carried out. In other words, the cytoskeleton is found to behave very much like a viscous polymeric 'fluid' (reviewed in Ref. [10]).

The isotropy, fluidity and reactivity of the amoeboid cytoskeleton has been the basis for a simple continuum model using the ideas of two-phase flow. The basic idea is that actin polymers can be regarded as a highly viscous polymeric fluid and that the aqueous portion of the cytoplasm can be regarded as another 'interpenetrating' fluid. Mathematical simulations with such models [13] have

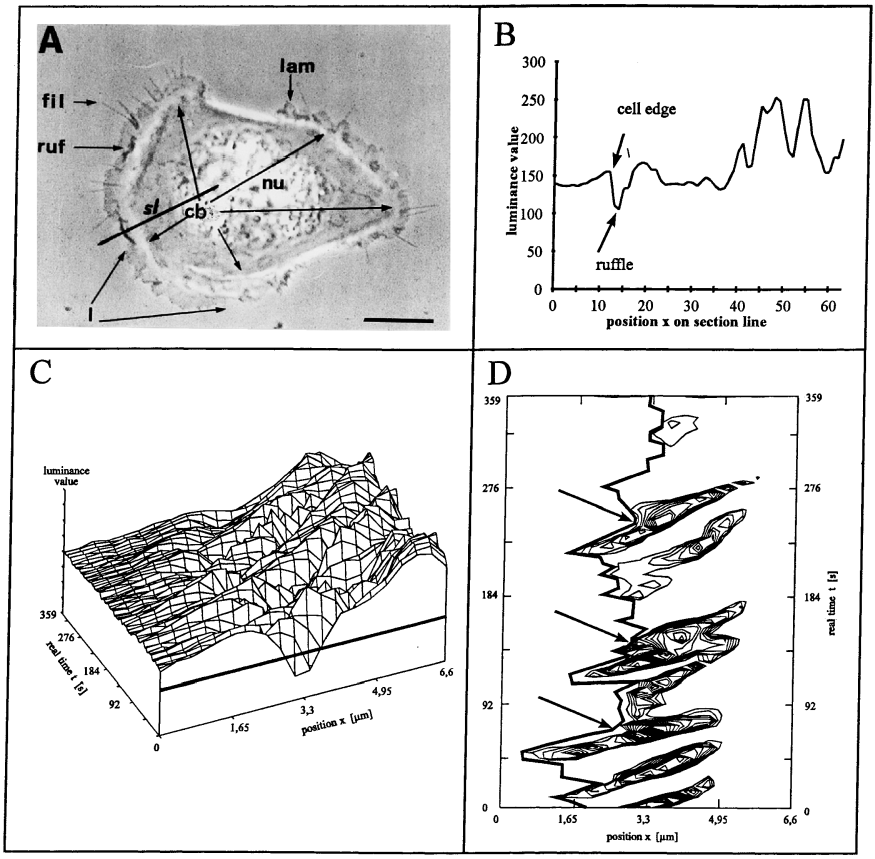

Fig. 1. Evaluation of phase-contrast video-images showing the protrusion–retraction dynamics at the periphery of an adherent (human epidermal) keratinocyte. (A) Steep edges of the 3-dimensionally extended cell body (cb) containing the nucleus (nu), are characterized by a bright halo (cb-arrows) which at two places coincide with the cell margin appearing stretched there, whereas elsewhere it is surrounded by a broad and flat lamella (1). At their tips there may extend filopods (fil) or lamellipods (lam), and often so-called 'ruffles' (ruf). *bar*: 10 µm. (B) Ruffles are detected as dark structures of relatively low luminance as seen in the 1-dimensional plot along a section line drawn over the picture in (A), starting with $x = 0$ outside the cell and crossing cell edge and lamella until reaching the cell body near $x = 40$ sample points. (C) Composite plot of luminance profiles as in (B) for increasing times t over 6 min. Moving valleys of low luminance, whose topographical lines below a certain threshold are plotted in (D), describe the more or less regular appearance of 'ruffles' at the retracting cell edge (lamella tip, whose motion in time is drawn as a bold line). Their centripetal movement has quite a constant speed (of about 5 µm/min), continuing even when the lamella tip extends again. (From Ref. [2].)

revealed that *without* boundary interactions an isotropic reactive the polymer fluid tends to generate irregular streaming patterns. These bear some similarity to the chaotic 'flares' observed in isolated cytoplasmic extracts of *Amoeba*

proteus [22]. In contrast, by including boundary interactions it is possible to produce models in which the cytoplasm undergoes predictable and sustained motions. This was shown in the case of the regular 'fountain streaming' found in amoeboid motion [9] and in modeling studies of the precise cytoplasmic flow and cortical deformation during the first cleavage division of the sea urchin egg [17,18].

In the case of adherent cells, for example keratinocytes, an essential new feature is introduced due to contact with the substratum and the production of traction [2,25]. In particular, cells that are almost radially symmetric are best suited for a detailed analysis of cell motility, see Fig. 1. The cell has a 'fried egg' morphology and the center is essentially stationary but the outer periphery of the lamella undergoes continuous cycles of stereotypical motility. Time series analysis of long video records of such keratinocytes reveal that lamellipodial protrusions at the cell periphery are quite periodic with period of $T \approx 2.5$ min. In addition, one-dimensional spatio-temporal correlation analysis along rays passing through the cell border yields a similar periodicity for so-called 'ruffle waves', see Fig. 1(B)–(D). These waves originate during the retracting phase of the cell margin along broad fronts (typically the wave front is 10 or 20 μm wide). The ruffle waves have a wavelength that is only a micron. The front propagates normal to its long dimension towards the nucleus at a fairly uniform rate of about 5 μm/min. The wave speed seems to be independent of the extension retraction cycle of the tip of the lamella. In other words, the ruffle continues to go centripitally even after the tip has stopped retracting and is again extending. Side-view electron micrographs of active lamellipods indicate that ruffle waves represent thickenings of the lamella which are filled with high concentrations of F-actin.

Further studies of the keratinocyte and other similar tissue cells have demonstrated a general and preexisting steady motion of cytoplasmic filaments directed from the outer periphery towards the cell body (this is the so called centripetal flow). The speed of this flow is very close to the speed of moving ruffles [15,16,2], and as a result one may presume that propagation of ruffles is simply another manifestation of this general cytoskeletal current. Hydrodynamic shear between the centripetal current and adhesive sites on the ventral surface of the cell could be sufficient to provide the traction stresses necessary for extension and flattening of the lamella. On the other hand one should remember that such a continuum viewpoint is simply a way of reformulating the average effects of large numbers of highly specific adhesive interactions between the cell and the substratum.

In this paper we present a new, simple derivation of our two-phase flow model, which we already have used for several applications [13,11,9, 10,23,6,19,4]. The new derivation has the advantage of reducing the required hypotheses to a minimal set of rules for the mechanics and kinetics of the F-actin polymer system. Indeed, a general minimization principle for the loss

of 'kinematic energy' is proposed which, in addition, allows to compute and visualize, in which parts of the cell lamella kinematic energy is gained or dissipated, and how the resulting cell translocation force depends on the mechano-chemical parameters. More details can be found in a further general article by the authors [3].

2. General two-phase flow model for the cytoplasm: model derivation

In accordance with previous model derivations [12,8,1], the actomyosin polymer network is thought to constitute the so-called *filament phase* which, in the continuum limit, has a volume fraction $\theta = \theta(t,x)$ at time t and at location x, and a corresponding mean velocity $v = v(t,x)$. Assuming a disassembly of filaments with rate η and a constant assembly rate $\beta < \eta$, we obtain $\theta_{eq} = \beta/\eta$ as the 'chemical filament equilibrium' and the following hyperbolic mass balance equation

$$\partial_t\theta + \nabla\cdot(\theta v) = \eta(\theta_{eq} - \theta). \tag{1}$$

Here we assume that the dissolved filaments units (e.g. G-actin monomers) are rapidly and uniformly distributed in the other, so-called, *solvent phase* with volume fraction $(1-\theta)$ and mean velocity $w = w(t,x)$. Then, if no net mass is produced in the system, the *total flux* of the two-phase fluid is divergence free:

$$\nabla\cdot(\theta v + (1-\theta)w) = 0. \tag{2}$$

Thus, for given time t and filament distribution $\theta = \theta(t,x)$ over $x \in \Omega = \Omega(t)$, a possibly time-dependent spatial domain, this divergence relation is the necessary incompressibility side condition for determining the two-phase flow velocities v and w, which in the assumed case of negligible inertia is most easily performed by just *minimizing* the following 'power functional' J. As usual, it is an integral over Ω computing the *net loss rate* of *kinematic energy* in the creeping flow as the difference between energy dissipation rate and energy gain rate:

$$J[v,w,p] := \frac{1}{2}\int_\Omega \nabla v\tilde{M}\nabla v + \Phi\theta|v|^2 + \varphi\theta(1-\theta)|v-w|^2 + \nabla w\tilde{M}_s\nabla w \tag{3}$$

$$-\int_\Omega \theta p_f\nabla\cdot v + (1-\theta)p_s\nabla\cdot w + p_{fs}(v-w)\cdot\nabla\theta. \tag{4}$$

where we used the tensor notation (e.g. for the 2-dimensional case) $\nabla v\tilde{M}\nabla v := \mu|\nabla v|^2 + \lambda(\nabla\cdot v)^2 + \nu|rot v|^2$.

The positive terms (3) describe energy dissipation due to internal viscosity (M) or external friction (Φ) of the filament phase and due to an interphase frictional drag (φ), as well as (a relatively small) viscosity (M_s) of the solvent

phase. Substracted from these terms are the other integral terms (4) that describe the *net rate of energy gain* due to stresses or pressures deforming the two-phase configuration. Here we model the so-called *static contractile stress* (a negative pressure) in the filament phase as

$$-p_{\mathrm{f}} = -P_{\mathrm{f}}(\theta) = \Psi(\theta) := \frac{\psi}{2}\theta \exp(-\theta/\theta_{\mathrm{sat}}), \tag{5}$$

the *static swelling pressure* in the solvent phase as

$$p_{\mathrm{s}} = P_{\mathrm{s}}(\theta) := \sigma \frac{|\ln(1-\theta)|}{1-\theta} \tag{6}$$

and the *static interphase pressure* as

$$p_{\mathrm{fs}} = P_{\mathrm{fs}}(\theta) := -\frac{\sigma}{1-\theta}. \tag{7}$$

Places where the integrands in Eq. (4) are positive indicate local energy gain, e.g. for the first term, if the filament network contracts and induces a negative divergence $\nabla \cdot v$. For further interpretation of these terms see Ref. [3].

However, as soon as the two-phase fluid starts to flow, we have to account for an *effective hydrostatic pressure* $p = p(t,x)$ which is added as a free variable to all the static pressures, i.e. $p_{\mathrm{f}} = p + P_{\mathrm{f}}(\theta), p_{\mathrm{s}} = p + P_{\mathrm{s}}(\theta)$ and so on. This yields an additional *Lagrange multiplier* term $-\int_\Omega p\nabla \cdot (\theta v + (1-\theta)w)$ in Eqs. (3) and (4), thus becoming a functional $\tilde{J} = \tilde{J}[v,w,p]$ also depending on the free pressure variable p. Standard arguments reveal that the augmented functional $\tilde{J}$ is of '*saddle point*' type, at least for variations of test functions $v, w, p \in L^2(\Omega)$, and that the stationary saddle point (v, w, p) satisfies the divergence relation Eq. (2). Moreover, assuming negligably small solvent viscosity ($M_{\mathrm{s}} = 0$) the effective hydrostatic pressure p obeys *Darcy's law* for the two-phase flow,

$$\nabla p = \varphi\theta(v - w) \tag{8}$$

with drag coefficient φ. For a full derivation and further explanations cf. [3]. Proceeding as in compressible fluid dynamics, namely solving for w and replacing it in Eq. (2), together with the variational equation for v provides the following linear elliptic system (generalized Stokes equations):

$$\nabla \cdot (\widetilde{M\nabla} v) - \nabla(\bar{P}(\theta) + p) = \Phi\theta v \tag{9}$$

$$\nabla \cdot \left(\frac{1-\theta}{\varphi\theta}\nabla p - v \right) = 0, \tag{10}$$

where the 'averaged two-phase pressure' is defined as

$$\bar{P}(\theta) = \theta \cdot P_{\mathrm{f}}(\theta) + (1-\theta) \cdot P_{\mathrm{s}}(\theta) = -\theta \cdot \Psi(\theta) + \sigma \cdot |\ln(1-\theta)| \tag{11}$$

Here we again used the tensor notation (e.g. for the 2-dimensional case) $(\widetilde{M\nabla} v) := \mu\nabla v + \lambda(\nabla \cdot v)I + v\, rotv\, I^{\perp}$ with I denoting the unit tensor.

So far, this model constitutes a *viscous, reactive and contractile two-phase fluid* satisfying the hyperbolic–elliptic system of differential equations (1), (9) and (10) in a possibly time-varying domain $\Omega(t)$ that might represent, for example, the projected 2-dimensional cytoplasmic region of a cell. It describes only intracellular microscopic interactions between filaments within the actomyosin network as well as between these filaments and solvent molecules. The only exception concerns the friction term Φ which is supposed to model interactions of actin filaments with transmembrane proteins that might adhere to the substratum underneath the domain $\Omega(t)$. Though, in general, the adhesion bonds follow a time dependent kinetics, we assume here, for simplicity, a constant *adhesive friction coefficient* Φ.

However, we also have to consider mechano-chemical interactions of the two fluid phases at different parts of the boundary $\partial\Omega$. Now, let $\Omega = \Omega(t)$ represent the flat lamella region that extends from a resting but active cell, see Fig. 2. This region could have three different types of boundaries, Γ_C, Γ_B and Γ, where we suppose, with n denoting the outer normal vector:

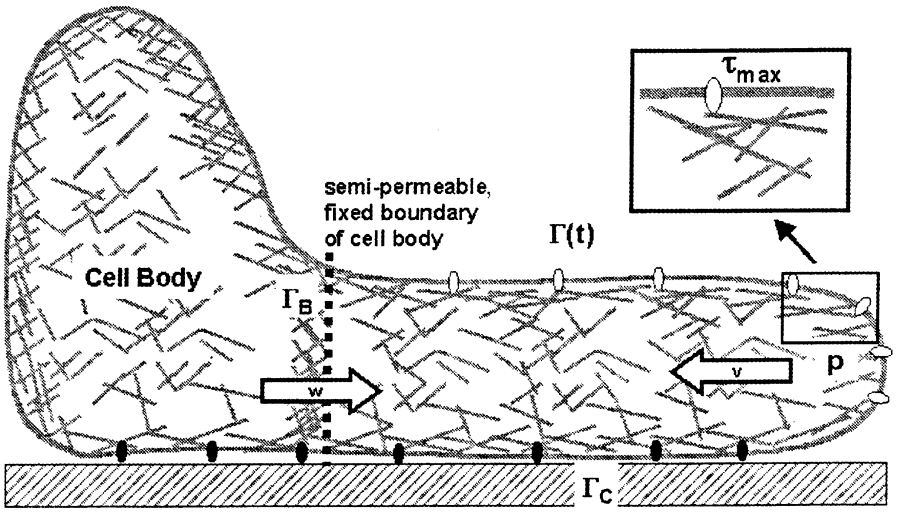

Fig. 2. Sketch of a 2-dimensional cross-sectional model for the two-phase flow dynamics of a cellular (pseudopod or) lamella. It is represented by a time variable domain $\Omega(t)$ with three boundaries: a fixed boundary Γ_C, where the lamella touches a substratum expressing adhesion proteins; another fixed but semi-permeable boundary Γ_B, where the actin filaments are connected to the stable cytoskeletal cortex of the cell body, while the solvent can pour through with velocity w; finally, a free boundary $\Gamma = \Gamma(t)$ constituting the cortical membrane–protein complex surrounding the lamella. The dynamics at the free boundary is determined by a force balance between hydrostatic pressure p and tension τ of the actin filament network that might be pulled with inward velocity v.

- at an 'obstacle', i.e. a *fixed impermeable boundary* Γ_C, the conditions $n \cdot w = 0$ for the solvent flow and $n \cdot v = 0$ resp. $n \cdot v \leqslant 0$ for the filament flow, depending on whether the filaments sticks to the boundary or not;
- at the 'cell body boundary', i.e. a *fixed permeable boundary* Γ_B that allows solvent molecules to pass with a certain drag resistance φ_B (but the filaments to stick), the condition $n \cdot v = 0$ and an additional boundary integral term for energy dissipation in the power functional J, Eqs. (3) and (4), namely $\int_{\Gamma_B} (1-\theta)(\frac{1}{2}\varphi_B (n \cdot w)^2 + P_B (n \cdot w))$, where P_B denotes a given 'outer pressure' inside the cell body;
- at a *free impermeable moving boundary* $\Gamma = \Gamma(t)$ the condition $n \cdot (v - w) \leqslant 0$, meaning that the normal filament velocity might be less than the moving boundary speed $\dot{\Gamma} = n \cdot (\theta v + (1-\theta) w)$ (i.e. $n \cdot v < \dot{\Gamma}$ defining the case of *filament disruption* from the lamella tip) or equal ($n \cdot v = \dot{\Gamma}$, the case of *filament attachment*), plus a further boundary integral term in the functional J, namely $-\int_\Gamma \tau_\Gamma n \cdot (v - w)$, where τ_Γ models the maximal tension under which filaments can sustain their sticky bonds to membrane proteins.

Given this model framework for interactions at the boundaries, we then have to solve the following *variational inequality problem*, namely to find functions $v, wH^1(\Omega)$ and $p \in L^2(\Omega)$ satisfying these boundary conditions such that local variations lead to non-negative differential increase of the Lagrange functional $\tilde{J}$, i.e. $D\tilde{J} \geqslant 0$. It can be shown, for sufficiently smooth boundaries, that this problem has a unique weak solution, at which the original energy loss functional J attains its global minimum in the above defined function subspace, for more details see Ref. [3]. Again, standard variational principles can be applied to obtain, in addition to the derived differential equations in the interior of the domain Ω, a set of (natural) boundary conditions for the flow velocities v and w as well as for the hydrostatic pressure p, provided the solutions are smooth enough. Besides the usual tangential Neumann conditions we get the following normal force balances, again for vanishing M_s,

- on Γ_B the porous flow law for the solvent yielding a boundary condition for the solvent pressure $-(\varphi_B/\varphi\theta)(n \cdot \nabla p) = p + P_s(\theta) - P_B$;
- on the free boundary Γ an equilibrium between the normal component of filament tension $\tau := n \cdot \widetilde{M\nabla} v \cdot n - \theta(p + P_f(\theta)) = (1-\theta)(p + P_s(\theta))$ and the solvent pressure, as well as the (envisaged) inequality condition $\tau \leqslant \tau_\Gamma$ and the Neumann inequality $(1/\varphi\theta) n \cdot \nabla p \leqslant 0$.

Altogether we can show that this linear elliptic (free) boundary value problem for determining v and p is well-posed, depending, for fixed time t, on the filament distribution $\theta(t,x) > 0$ in the interior Ω and smoothly approaching the boundaries. Notice that the hyperbolic equation (1) for θ requires the boundary condition $\theta = 0$ at boundary points of 'disruption'. Moreover, in a point of 'attachment' at the free boundary, we have $\dot{\Gamma} = n \cdot v$ and $n \cdot \nabla p = 0$, whereas a point of 'disruption' is characterized by the conditions $\theta = 0, \tau =$

$\tau_\Gamma = 0, p = 0$ and $\dot{\Gamma} = n \cdot v - (1/\varphi\theta) n \cdot \nabla p > n \cdot v$. The boundary conditions for $(1/\theta) n \cdot \nabla p$ have to be understood in a suitable limit from the interior of Ω.

3. Periodic and chaotic waves for a one-dimensional fixed domain

3.1. Assumptions

For exploring the dynamical properties of the presented two-phase flow model let us restrict our analysis and numerical simulations to the one-dimensional case. Then, viscosity of the filament phase can be simply characterized by a scalar coefficient $M(\theta) = \mu \cdot \theta$, and the interior flow dynamics of the hyperbolic–elliptic system equations (1), (9) and (10) is mainly determined by the following two 'state functions' of the actin polymer fluid, namely the linear *chemical assembly rate* $R(\theta) = \eta \cdot (\theta_{eq} - \theta)$ and the non-linear *mechanical stress rate* $S(\theta) = -\bar{P}(\theta)/\mu = \theta \cdot \Psi(\theta)/\mu + (\sigma/\mu) \ln(1 - \theta)$.

As depicted in Fig. 3, for small as well as for higher filament concentrations θ, we observe a decreasing stress rate, $S'(\theta) < 0$, and the mechanical system is in its *swelling regime*. For intermediate concentrations, $\theta_* < \theta < \theta^*$, we have

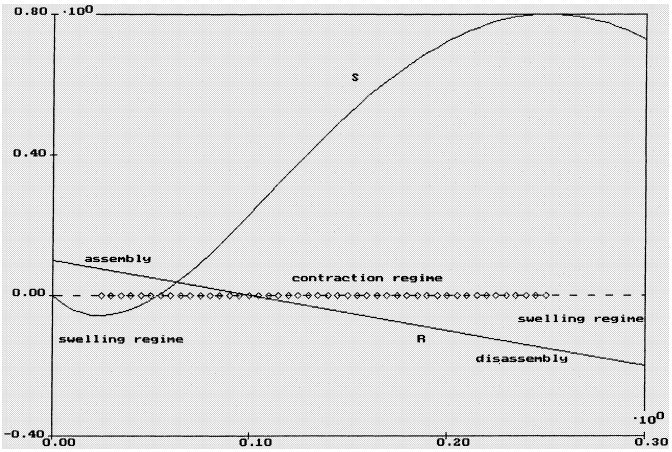

Fig. 3. Plot of the two rate functions (over filament concentration θ) determining the two-phase flow dynamics, namely the linear chemical assembly rate $R(\theta)$ and the mechanical stress rate $S(\theta)$, see definitions in the text. At lower concentrations ($\theta < \theta_{eq} = 0.1$) ATP-dependent energy is consumed for assembly of actin filaments. The relatively sparse network tends to swell and dissipate energy ($S'(\theta) < 0$ for $\theta < \theta_*$) defining a *swelling* 'sol' state; whereas for intermediate concentrations ($S'(\theta) > 0$ for $\theta_* < \theta < \theta^*$) defining the *contraction* regime, energy is consumed for mutual attraction of actin filaments by APT-dependent action of myosin polymers. For even higher concentrations ($S'(\theta) > 0$ for $\theta > \theta^*$) contractility is inhibited and dominated by dissipative *swelling* of the condensed 'gel'.

$S'(\theta) > 0$ meaning that an increasing filament concentration would induce more net contractile stress thus defining the *contractile regime*.

Therefore, the condition $S'(\theta_{eq}) > 0$ at chemical equilibrium implies that, when initially starting with a homogeneous filament distribution, i.e. $\theta = \theta_{eq}$ and $v = 0$, a spontaneous instability arises in the linearization of the hyperbolic system. For instance, let us consider a *fixed* interval $\Omega = [0, L]$, which could, as a one-dimensional model, describe the in vitro situation of cytoplasm extracts in a cuvette [14], with sticky boundary at $x = 0$ and non-sticky boundary at $x = L$, both impermeable for the solvent.

3.2. Results

The mechanical instability leads, for $t > 0$, to a sudden disruption of the actin filaments from the boundary $x = L$ and subsequent formation of a retracting wave moving towards the sticky boundary $x = 0$.

For positive drag $\varphi > 0$ or adhesive friction $\Phi > 0$ this wave develops an increasing peak of higher filament concentration moving as a growing travelling wave, eventually being absorbed into the (already present) peak at $x = 0$. For quite a large range of parameters a completely periodic solution results by repetitive disruption and wave formation with period T in the order of minutes, see Fig. 4. This reproduces the experimental observations mentioned above, [14,21], and supports as its underlying mechanism a chemo-mechanical *cycle of disruption–contraction–relaxation–reassembly*. Also, these repetitive contraction waves resemble the observed 'ruffles' arising at the lamellipodial tip and being retracted towards the cell body, compare Fig. 1. This in vivo modelling situation with moving boundary is treated in the next section.

Even for the simpler case of fixed boundaries, our numerical simulations confirm earlier results of two-dimensional computations which had produced spatio-temporally irregular or chaotic solutions [13].

First, when increasing the interphase drag, $\varphi > 0$, or the adhesive friction, $\Phi > 0$, or when decreasing contractility, Ψ, the waves intensify in amplitude but simultaneously slow down (their period increasing $T \approx 2.0$), until they do not reach the left hand boundary any more, rather attain an oscillating location in-between (see Fig. 5(a)). However, as the disruption–contraction–relaxation cycle from the right hand boundary continues, we again observe periodic solutions but with double period $T = 4.0$ (see Fig. 5(b)) or, sometimes, quasiperiodic behavior with an obvious spatial coupling of two periodic oscillators near both boundaries.

Second, when increasing the swelling rate, σ/μ, in comparison to the contraction rate, ψ/μ, so much that the swelling actin network pushes against the non-sticky boundary $x = 1$, then we observe quasi-steady solutions with contracting filament peaks at both boundaries, see Fig. 6. Apparently, this non-symmetric configuration is unstable as it happens that a growing local

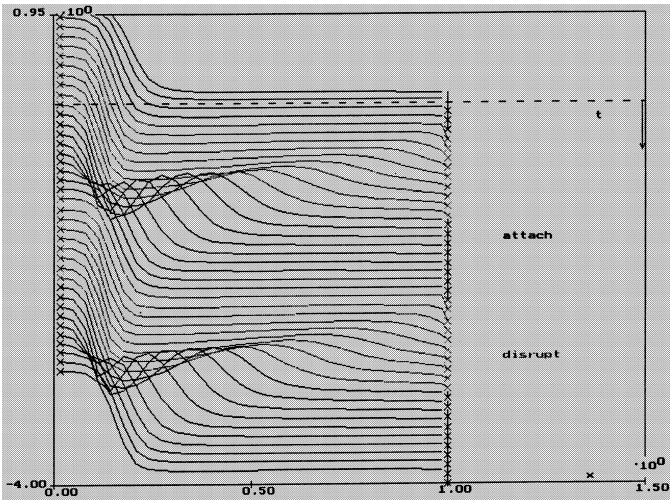

Fig. 4. Simulations of repetitive contraction waves in a 1-dimensional two-phase flow model on a fixed domain $\Omega = [0,1]$ with sticky boundary at $x = 0$ and non-sticky boundary at $x = 1$. Plot of actin filament concentration $\theta = \theta(x,t)$ for t from 0 to 4 min (drawn from back to front) showing periodic filament disruption, wave initiation, and subsequently, new filament attachment at $x = 1$. The period is $T \approx 1.8$ min relative to an assumed actin assembly rate of $\eta = 1/\text{min}$. Biomechanical parameters are filament viscosity $\mu = 0.1$ kPa min, contractility $\psi = 25$ kPa, saturating concentration $\theta_{\text{sat}} = 0.2$, swelling coefficient $\sigma = 0.5$ kPa, drag $\varphi = 0.01$ and adhesive friction $\Phi = 0.26$, both in kPa · min/μm^2.

instability arises in the central region with lowest filament concentration, forming a slowly varying wave eventually moving in one or the other direction and finally being attracted by one of the boundary peaks (Fig. 6(a) and (b)). Longer simulations reveal irregular behavior with no apparent periodicities, so that we conjecture to observe chaotic wave behavior (Fig. 6(c)).

4. One-dimensional dynamics of lamellipodial protrusion and retraction

4.1. Assumptions

In order to model the in vivo situation of lamella formation and its dynamics around the periphery of adhering cells, let us again restrict the analysis to the one-dimensional case, thereby trying to match the experimental data evaluation along transversal rays (see Fig. 1(C) and (D)). For this purpose let $\Omega(t) = [0, L(t)]$ describe the cross-sectional region of a lamella, with $x = 0$ corresponding to the fixed cell body boundary Γ_{B}, permeable only to solvent molecules, and with $x = L(t)$ denoting the tip of the lamella as a free impermeable moving boundary Γ. Since the cortical cytoskeleton of the cell body is

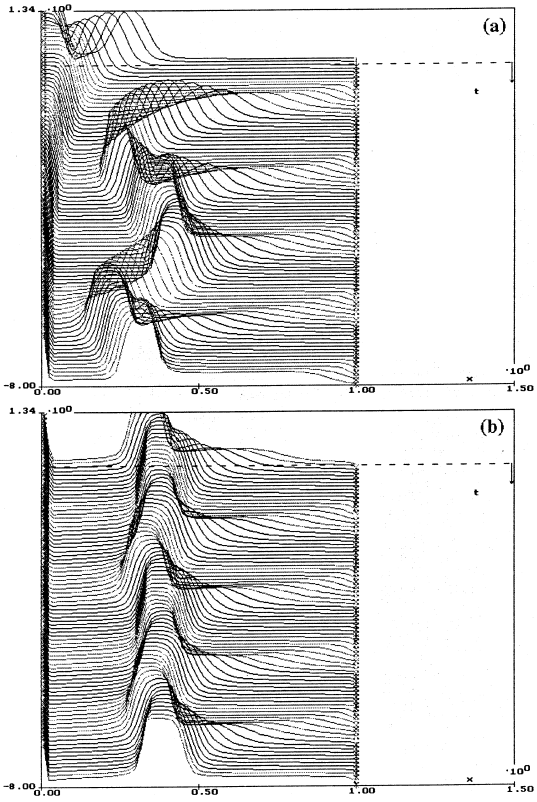

Fig. 5. Irregularities in the periodic contraction–relaxation cycle (Fig. 4) appearing e.g. when the adhesional friction is increased, here $\Phi = 0.32$. Then the filament contractility is more localized leading to higher peak concentration in the waves, and eventually, to failure of its attraction by the fixed actin peak at $x = 0$, see (a), plots extending over 8 min. The 'intermediate' actin wave may stagnate but (quasi-) periodically move to the right or left trying to capture the period of repetitive wave disruptions occuring at $x = 1$, whose period $T_{\text{wave}} = 2.0$ min is longer than before and half the overall period of $T = 4.0$ min, see (b).

assumed to have similar consistency as the filamenteous actin network at $x = 0$ with $\theta_B = \theta(x = 0)$, we suppose there a constant pressure $P_B := P_B - P_s(\theta_B)$ now denoting the hydrostatic pressure that exceeds the swelling pressure of the cytoskeleton. Thus, with $\varphi_B = 0$, we require the Dirichlet condition $p = P_B$ at $X = 0$ for the hydrostatic pressure p in the lamella.

The condition for 'attachment' of actin filaments to membrane proteins at $x = L(t)$ means that the local filament network tension is subcritical, $\tau(x, t) \leqslant \tau_\Gamma$, where the maximal tension $\tau_\Gamma = \tau_{\max} \cdot \theta_\Gamma/(K_\tau + \theta_\Gamma)$ is modelled to be proportional to the number of membrane proteins bound by actin filaments: corresponding to their mean length and diffusional activity radius, we take θ_Γ as the

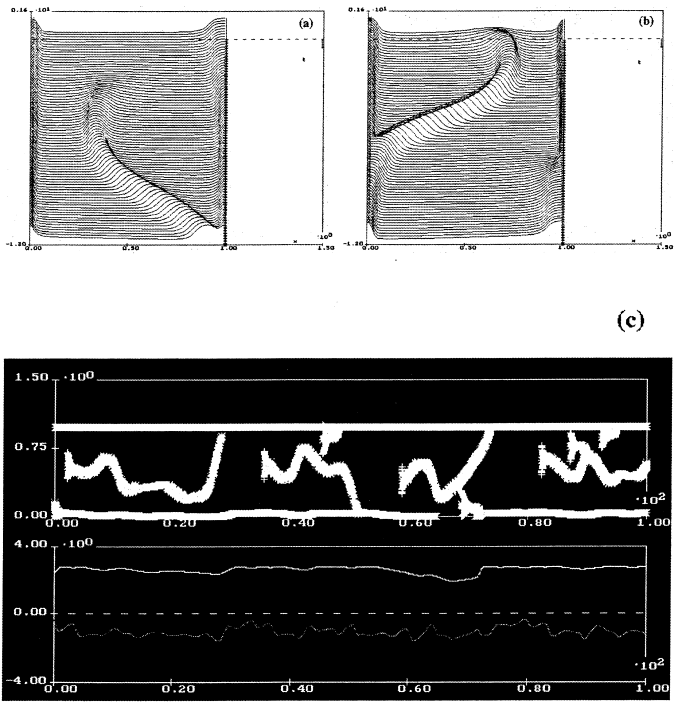

Fig. 6. Unstable quasi-symmetric solutions of the two-phase flow model, occuring if swelling ($\sigma = 0.7$ kPa) is enlarged. Then the actin filaments are pushed against both sides of the fixed interval, however, wave instabilities occur in the relatively low concentrated middle region: plots (a), (b) extending over 10 min. Longer time simulations reveal irregular (possibly chaotic) wave patterns shown by the long term plots in (c) of actin concentration $\theta(0,t)$ and tension $\tau(0,t)$ (lower panel) as well as of the local actin concentration maxima in the interval $[0,1]$ (upper panel) plotted over time, from 0 to 100 min.

average of filament concentration θ over a boundary region $L(t) - d_\tau \leqslant x \leqslant L(t)$, e.g. with $d_\tau = 0.03 \cdot L_0, L_0$ denoting the mean basic lamella length of about 2 μm.

4.2. Numerical solution techniques

Let us briefly describe the numerical algorithms that we use for our computer simulations. As in the fixed case $\Omega = [0,1]$, for any given discrete time t the filament concentration $\theta = \theta(x,t)$ is approximated by a piecewise constant function on n (e.g. $= 31$) interior compartments. Then, given this distribution, the (pseudo-)stationary linear elliptic system in Eqs. (9) and (10) with appropriate boundary conditions is solved by an alternating iteration procedure with (tridiagonal) matrix inversion to obtain a piecewise linear approximation for the

filament velocity $v = v(x, t)$ and a piecewise constant approximation for the pressure $p = p(x, t)$. At the free boundary $x = L(t)$, the lamella tip, we first *(case I: attachment)* search for solutions satisfying the homogeneous Neumann condition $\partial_x p = 0$ and accept it if $\tau \leqslant \tau_\Gamma(\theta_\Gamma)$, i.e. if the pressure at the lamella tip fulfils the inequality $p \leqslant p_{\max} := (1/(1-\theta))\tau_\Gamma(\theta_\Gamma) - P_s(\theta)$; otherwise *(case II: disruption)* we declare that the filament network has been disrupted from the lamella tip and search for solutions satisfying the homogenous Dirichlet condition $p = 0$ at $x = L(t)$. Then, after having checked the (discretized) inequality $\partial_x p \leqslant 0$ there, the current speed $\dot{L}$ of the free boundary is calculated as defined in Section 2. In *(case I: attachment)* with $\dot{L}(t) = v(L(t), t)$ we transform the domain $[0, L(t)]$ to the standard fixed interval $[0, 1]$ and apply there, as we did for the fixed domain in the last section, the upwind difference Euler step in order to solve the now transformed hyperbolic Eq. (1). In *(case II: disruption)* we first proceed in the same way obtaining the filament distribution θ on an interval $[0, \tilde{L}(t)]$ having moved along the characteristic curve locally defined by $\dot{\tilde{L}}(t) = v(\tilde{L}(t), t)$ with initial condition $\tilde{L} = L$ at time t. Afterwards the really extended length of the lamella after $\mathrm{d}t$ is determined via the simple Euler step $L(t + \mathrm{d}t) = \tilde{L}(t + \mathrm{d}t) + (\dot{L}(t) - v(L(t), t) \cdot \mathrm{d}t$, and the filament distribution in the newly covered lamella area is adjusted from zero to the newly assembled concentration level $\theta = \eta \cdot \theta_{\mathrm{eq}} \cdot \mathrm{d}t$. Thus, the iteration cycle is closed and we restart with $t := t + \mathrm{d}t$.

4.3. Results

Initially starting with a lamella in the constant equilibrium state $\theta = \theta_{\mathrm{eq}}$ the free lamella tip will, in general, always move, either by shrinking due to contraction or by extending due to protrusive pressures. However, under parameter constellations similar to those in the last section, numerical simulations show the already described disruption of actin filaments from the lamella tip and the formation of a retracting wave. Again, depending on the choice of the mechanical parameters, the lamella tip will retract or extend: In Fig. 7(a) we show a particular simulation, where the lamella tip comes to rest as soon as the backwards travelling contraction wave has arrived at the fixed 'cell body' boundary $x = 0$; afterwards the tip very slowly extends until, for long time, it stabilizes leading to a *stable stationary actin filament distribution* $(\theta = \theta(x))$, which decreases from a fixed 'gel concentration' at the 'cell body' down to zero at the lamella tip, see Fig. 7(b). In this steady state, which might model the stable lamella of fast moving keratocytes [25], there is ongoing reassembly of actin filaments at the anterior lamella region, from where they are transported towards the cell body by the 'centripetal' actin flow. The strength of this contractile flow $(|v|)$ and the lamella length adjust in such a way, that the locally induced drag in the two-phase fluid is equilibrated by the pressure drop (p) from an imposed hydrostatic pressure $P_B > 0$ at the cell body down to zero at the lamella tip.

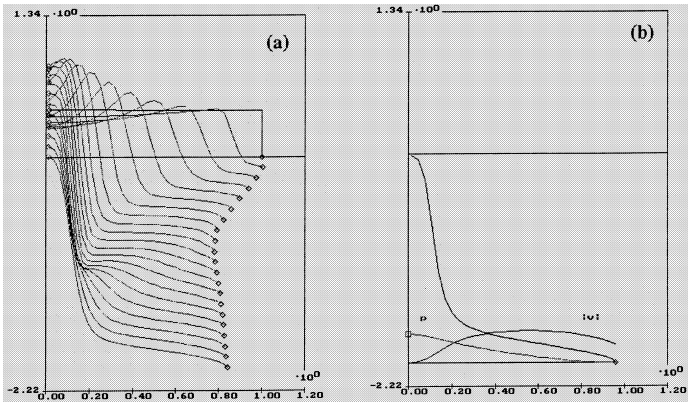

Fig. 7. Simulations of the 1-dimensional contractile two-phase flow model with fixed sticky boundary (but permeable for the solvent) at $x = 0$ and free boundary $x = L(t)$. (a) Actin filament concentration $\theta = \theta(x, t)$ is plotted for increasing times from back to front, extending over 2 min. Parameters are $\psi = 18$, $\sigma = 0.25$, $\varphi = 0.008$, $\Phi = 0.4$, with relatively low cell body pressure $P_B = 0.25$ Pa, and tension threshold $\tau_{max} = 30$ Pa with saturation constant $K_\tau = 0.1$. For times $t \to \infty$ the concentration profile stabilizes and the lamella length converges to a value $L_\infty \approx 0.97$. (b) The stable steady state distribution of $\theta(x)$ (upper curve), the modulus $|v(x)|$ of the centripetal filament velocity and the hydrostatic pressure $p(x)$.

This situation can occur provided the filament concentration near the tip (θ_Γ) is too small to form enough connections to membrane proteins, and the induced filament tension τ at the tip (due to contractile and viscous stresses) is supercritical so that attachment cannot happen. Indeed, when lifting the critical tension τ_{max} a bit, we observe sudden attachment and subsequent contraction of the whole lamella, see Fig. 8(a). However, due to the rapidly increasing filament concentration at the retracting tip the filament stress becomes supercritical again, with subsequent filament disruption and tip stagnation. Continuing the simulations we would observe a repetition of this contraction–relaxation cycle but with the lamella gradually decreasing in length. Therefore, in order to balance the mean contractile action of the actin polymer system and sustain a sufficient protrusion length, we have to provide a counteracting protrusion force, for example, by increasing the cell body pressure P_B. Indeed, for the parameters chosen in Fig. 8(b), very similar as in the fixed boundary situation (see Fig. 4), we obtain a periodic cycle of alternating disruption and attachment of the actin filaments, now exactly timed with alternating protrusion and retraction of the lamella. By changing the mechanical parameters slightly, the amplitude of these protrusion–retraction dynamics can be enlarged, e.g. by a further increase of the tension threshold τ_{max} leading to longer periods of contraction, balanced by an increasing protrusive pressure at the lamella tip due to lowering the interphase drag, φ, see Fig. 9(a). Notice, the periodic contraction waves that are initiated at the

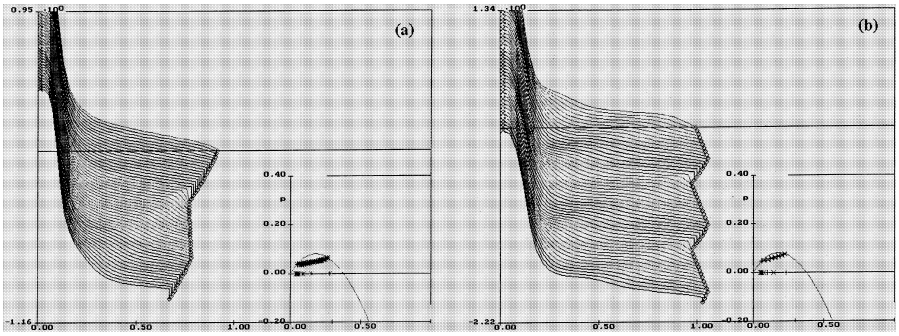

Fig. 8. Continuation of the simulation in Fig. 7(b): (a) Sudden increase of the tension threshold ($\tau_{\max} = 35$ Pa) leads to attachment of filaments at the free boundary $x = L(t)$ and its subsequent retraction, during which the filament concentration at the lamella tip gradually rises until, after about 0.3 min, filament disruption takes place. Thereafter the tip stagnates, while a slight shoulder of higher actin concentration moves centripetally towards $x = 0$; simultaneously, tension of network at the tip gradually relaxes until, after about 0.4 min, it again attaches. Then the process of tip retraction repeats. **Inset**: Curve plot of the maximal pressure $p_{\max}(\theta_\Gamma)$ that actin bonds to membrane proteins could sustain in case of attachment, given a filament concentration θ_Γ near the boundary; also plotted (*) are actual values of hydrostatic pressure p there: Periods of attachment start at the left side of the $p_{\max}$-curve and show increasing values of θ_Γ and p as long as $p < p_{\max}(\theta_\Gamma)$ is satisfied, whereas at the time of disruption the pressure p jumps down to zero and θ_Γ rapidly decreases until the process repeats with newly attachment. (b): Doubling cell body pressure ($P_B = 0.5$ Pa) extends the mean lamella length and induces a regular periodic cycle of lamella protrusion (during disruption of filaments) and retraction (during their attachment). Plot extends over 2 min, the period being $T = 0.8$ min, with $T_{\text{protrusion}} = 0.5$ and $T_{\text{refraction}} = 0.3$ min.

lamella tip every time disruption occurs, develop higher condensation of actin in its wave peak as the sufficiently strong adhesive friction, Φ, resists the backward motion of the cytoplasm. Thus, the theoretical plot in Fig. 9(a) qualitatively resembles the experimental plot in Fig. 1(c) though reversed, since there the waves describing 'ruffles' retracted towards the cell body are 'valleys' of dark luminance values. Also, the resulting characteristic quantities, as cycle period and retraction speed, are in the same range as the observed data, namely periods of about $T = 1$ min and speeds of about *one lamella length per min*.

4.4. Localization of energy gain and loss

From numerical simulations it turns out that *adhesive friction* Φ and *net contractile stress* S play the central roles in determining the relation between *input energy* and *output forces*, whereas viscosity μ determines the amount of *energy loss*. To remember, the modelled biomechanical system of 'creeping two-phase flow' is always in a pseudo-steady equilibrium characterized by

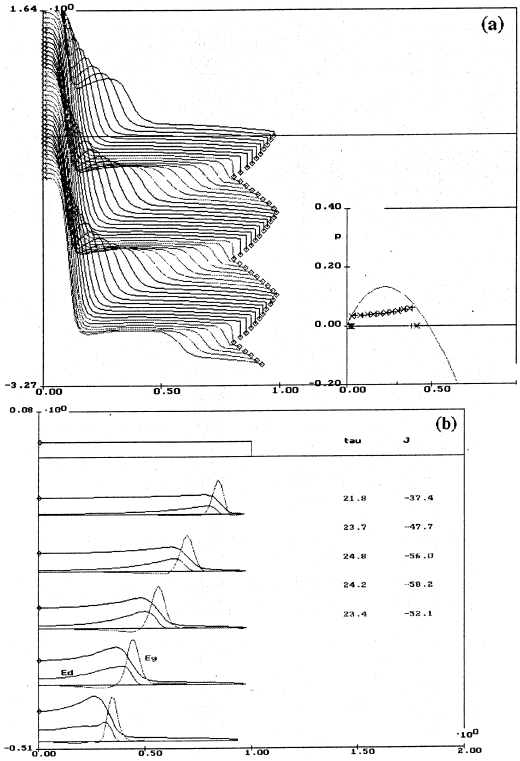

Fig. 9. Stable periodic protrusion–retraction cycle in the one-dimensional lamella model. (a): Plots similar as in Fig. 8(b), extending over 3 min, with slightly changed parameters ($\varphi = 0.005$, $\Phi = 0.35$, $P_B = 0.4$ Pa, $\tau_{max} = 38$ Pa) yielding a period of $T = 1.15$ min with $T_{protrusion} = 0.5$ and longer $T_{retraction} = 0.65$ min. The following pictures (b–d) show time shots in intervals of $\Delta t = 0.1$ min of the distribution of actin filaments $\theta(x, t)$ [upper curve], of local energy dissipation rate $E_d(x,t)$ (curve with hump to the left, scaling reduced by 1/10) and of local energy gain rate $E_g(x,t)$ [curve with hump to the right, scaling reduced by 1/50]. Also shown are the successive values of traction force τ_B at $x = 0$ and total energy loss rate J. (b) Development of a wave after initial disruption from the constant chemical equilibrium state, $\theta = \theta_{eq} = 0.1$. While energy dissipation E_d mainly appears at the wave concentration maximum, energy gain E_g always occurs 'behind the wave'. (c–d) Successive waves at later stages in the periodic cycle, during extension shortly after disruption (c) and during contraction (d). Actin gel concentration at $x = 0$ has a constant value of $\theta_B = 0.4$.

minimization of the power functional J calculating the 'total energy loss rate' summed up over the whole lamella domain $[0, L(t)]$. Now, in Fig. 9(b)–(d) we have plotted, for various situations within the protrusion–retraction process, the spatial distribution not only of the actin filament concentration, but also of the 'local energy dissipation rate' E_d and the 'local energy gain rate' E_g. In addition, we have calculated the induced *filament tension* τ_B at the cell body $x = 0$ and the value $J = \int_0^{L(t)} (E_d - E_g)$ of the minimized 'total energy loss

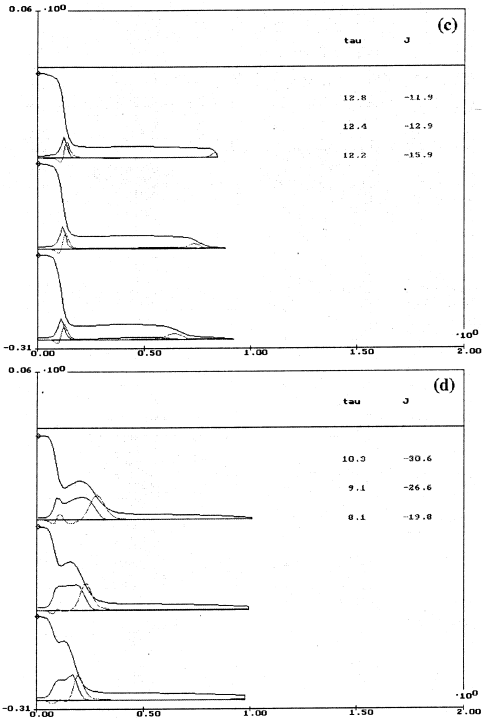

Fig. 9. Continued.

rate'. Here, E_d just collects all the integral terms in Eq. (3), but in spite of the choice of high adhesive friction, Φ, filament viscosity essentially dominates the friction and drag terms. On the other hand, E_g contains all integral terms in Eq. (4), but due to the choice of strong contractivity, ψ, energy gain is dominated by contractile energy which is put into the filamenteous network by the ATP-dependent action of myosin, however, damped by network swelling, σ.

Now, the striking observation is that energy gain E_g is exclusively localized to the region *behind the contraction wave*, whereas energy dissipation E_d is significant in all regions where the filament network is going to be compressed. Therefore, it seems as if the 'contraction wave' is actively pushed and compressed by forces in its wake: indeed, the most important and dynamically effective contraction takes place in this region, where actin filaments from the lower concentrated area at the tip are attracted by the higher concentrated shoulder or peak of the wave.

Finally, we have computed the *traction force* $\tau_B = \int_0^{L(t)} \Phi\theta|v|$ onto the cell body due to the frictional interaction of retracting acting filaments with

adhesion proteins connected to the substratum. This force is eventually responsible for and proportional to the rate of cell translocation towards the protruded lamella tip. During the periodic lamella cycle it increases to a maximal value ($\tau_B \approx 12.8$ Pa) at the moment of disruption, see Fig. 9(c), whereas it attains its minimal value ($\tau_B \approx 8.1$ Pa) when the contraction wave reaches the cell body, see Fig. 9(d). Simultaneously, the *net energy input* ($-J$), i.e. the difference between total energy input and total energy dissipation, is always positive meaning that we have negative entropy production, i.e. *entropy reduction*, in the active lamella therefore representing the typical feature of a 'biological motor'. It also varies cyclically but contrarily to the output force τ_B. After disruption, when the initiated contraction wave is flat, the net energy input is minimal ($-J = 11.9$ Pa), whereas it is maximal ($-J = 30.6$ Pa) as the increased wave is approaching the peak at $x = 0$.

Consistent with the formula for τ_B, the potential traction force for cell translocation is reduced, if we lower the adhesive friction (Φ). In parallel, a similar reduction of the net energy input ($-J$) occurs.

5. Discussion: the role of stochastics and outlook to further modelling

These various kinds of spatio-temporally solutions to the one-dimensional hyperbolic–elliptic boundary value problem seem to confirm that the presented two-phase fluid model, with its main non-linearity $S(\theta)$ in Fig. 3, has the capacity to produce a broad spectrum of dynamical behavior, already in the one-dimensional situation with fixed boundaries. Since the derived continuum equations approximate the stochastic 'biointeraction' between cytoplasmic filaments and proteins, they might serve as a suitable tool for proving that the observed richness in the dynamics of cellular motility could be due to the mechano-chemical properties of the cytoplasm.

So far, our 1-dimensional model for lamella dynamics assumed that the cell body (with its boundary $x = 0$ to the lamella) stays fixed while the lamella tip protrudes or retracts. The same assumption holds for a simplified circular model that describes tangential cytoplasm flow and radial lamella protrusions around the cell periphery, assumed to be a circle with fixed radius [5]. In an even more simplified model [23], deformations of cell body shape were considered, though directly dependent on local actin filament concentration which, by its varying distribution around the cell periphery, may induce a polarization of the cell. Indeed, many motile tissue or blood cells (as leukocytes or fish keratocytes) soon after displacement on a substratum polarize their shape by expressing one leading lamella that performs protrusions and determines the direction of locomotion, whereas the rear of the cell is characterized by cytoplasmic contraction.

One unresolved question is whether the experimentally observed fluctuations in direction and motile activity of the leading lamella can result from irregular or chaotic cytoplasm dynamics within the deterministic framework of continuum models as presented in this paper; or if they are the consequence of additional stochasticity effected by random fluctuations of the mechanical or chemical parameters. The latter hypothesis has been investigated in [23] assuming that actin polymerization is stimulated by membrane receptors which randomly diffuse and bind certain ligands. In this combined deterministic–stochastic model the resulting fluctuations of cell polarization and retrograde cytoplasmic flow induce corresponding fluctuations of the translocation vector, thus leading to typical cell migration paths which can be characterized as directionally persistent random walks.

Another important candidate for inducing stochasticity in cell motion is the process of formation and configuration of adhesion bonds, being essential for force transduction between cell and substratum. Hitherto stochastic models that took into account the kinetics, diffusion and transport of adhesion receptors in order to quantify the dynamics of adhesion and to determine the resulting cell translocation speed, see e.g. Ref. [24], lack in considering the internal cytoplasm dynamics or, at least, the feedback that it gets from the adhesion kinetics. Thus, we address this as a further open problem, namely to investigate hybride models which, for example, combine the presented two-phase flow model for the cytoplasm with stochastic models for the tension dependent kinetics of attachment/disruption between actin filaments and membrane proteins as well as the binding/disruption kinetics between adhesion proteins and the substratum; a first attempt is performed in Ref. [20].

Acknowledgements

Thanks are due to the Research Program SFB 256 'Non-linear Partial Differential Equations', Univ. Bonn, which has sponsered the collaboration between the authors, and to Boris Hinz who provided various figures. However, most thanks are given to Tanya Kostova and her friendly team for organizing the wonderful and effective Conference on Deterministic and Stochastic Modelling of Biointeraction in Sofia, August 1997.

References

[1] W. Alt, Biomechanics of actomyosin mediated motility of keratinocytes, Biophysics 41 (1996) 181.

[2] W. Alt, O. Brosteanu, B. Hinz, H.W. Kaiser, Patterns of spontaneous motility in videomicrographs of human epidermal keratinocytes (HEK), Biochemistry and Cell Biology 73 (1995) 441.
[3] W. Alt, M. Dembo, The dynamics of viscous reactive and contractile two-phase fluids, Biophys. J., submitted.
[4] W. Alt, V. Lendowski, Modelling and simulation of particle movement in reactive two-phase fluids, Preprint SFB 256, Univ. Bonn 540, 1998.
[5] W. Alt, R.T. Tranquillo, Basic morphogenetic system modeling shape changes of migrating cells: How to explain fluctuating lamellipodial dynamics, J. Biol. Systems 3 (1995) 905.
[6] W. Alt, R.T. Tranquillo, Protrusion–retraction dynamics of an annular lamellipodial seam, in: W. Alt, A. Deutsch, G. Dunn (Eds.), Dynamics of Cell and Tissue Motion, Birkhäuser, Basel, 1997, p. 73.
[7] L. Cao, Y. Wang, Mechanism of the formation of contractile ring in dividing cultured animal cells. II. Cortical movement of microinjected actin filaments, J. Cell Biol. 111 (1990) 1905.
[8] M. Dembo, Field theories of the cytoplasma, Comments Theoret. Biol. 1 (1989) 159.
[9] M. Dembo, Mechanics and control of the cytoskeleton in Amoeba proteus, Biophys. J. 55 (1989) 1053.
[10] M. Dembo, On free boundary problems and amoeboid motion, in: N. Akkas (Eds.), Biomechanics of Active Movement and Division of Cells, NATO ASI Ser. H84, Springer, Berlin, 1994, p. 231.
[11] M. Dembo, F.W. Harlow, Cell motion, contractile networks, and the physics of interpenetrating reactive flow, Biophys. J. 50 (1986) 109.
[12] M. Dembo, F.W. Harlow, W. Alt, The biophysics of cell surface mobility, in: F.W. Wiegel, A.D. Perelson, Ch. DelLisi (Eds.), Cell Surface Dynamics, Concepts and Models, Marcel Dekker, New York, 1984, p. 495.
[13] M. Dembo, M. Maltrud, F.W. Harlow, Numerical studies of unreactive contractile networks, Biophys. J. 50 (1986) 123.
[14] R.M. Ezzell, A.J. Brothers, W. Cande, Phosphorylation dependent contraction of actomyosin gels from amphibian eggs, Nature 306 (1983) 620.
[15] G. Fisher, P.A. Conrad, R.L. DeBasio, R.B. Taylor, Centripetal transport of cytoplasm, actin, and the cell surface in lamellipodia of fibroblast, Cell Motil. Cytoskeleton 11 (1988) 235.
[16] P. Forscher, H.L. Chi, C. Thompson, Novel form of the growth cone motility involving site-directed actin filament assembly, Nature 357 (1992) 515.
[17] X. He. M. Dembo. A dynamical model of cell division, in: W. Alt, A. Deutsch, G. Dunn (Eds.), Dynamics of Cell and Tissue Motion, Birkhäuser, Basel, 1997, p. 55.
[18] X. He, M. Dembo, On the mechanics of the first cleavage division of the sea urgin egg, Exp. Cell Res. 233 (1997) 252.
[19] V. Lendowski, A. Mogilner, Origin of actin-induced locomotion of listeria, in: W. Alt, A. Deutsch, G. Dunn (Eds.), Dynamics of Cell and Tissue Motion, Birkhäuser, Basel, 1997, p. 93.
[20] J. Lenz, W. Alt, M. Sahm, Model of adhesion kinetics and traction dynamics in cell locomotion, Manuscript, Univ. Bonn 1999.
[21] Thomas Pohl. Periodic contraction waves in cytoplasmic extracts, in: W. Alt, G. Hoffmann (Eds.), Biological Motion , vol. 89, Springer, Berlin, 1990, p. 55.
[22] D.L. Taylor, J.S. Condeelis, P.L. Moore, R.D. Allen, The contractile basis of amoeboid movement I. The chemical control of motility in isolated cytoplasm, J. Cell Biol. 59 (1973) 378.
[23] R.T. Tranquillo, W. Alt, Stochastic model of receptor-mediated cytomechanics and dynamic mophology of leukocytes, J. Math. Biol. 34 (1996) 361.
[24] M.D. Ward, D.A. Hammer, Focal contact assembly through cytoskeletal polymerization: steady state analysis, J. Math. Biol. 32 (1994) 677.

[25] R. Winklbauer, Andreas Selchow, Beate Boller, Jürgen Bereiter-Hahn, Embryonic mesoderm cells and larval keratocytes from Xenopus: Structure and motility of single cells, in: W. Alt, A. Deutsch, G. Dunn (Eds.), Dynamics of Cell and Tissue Motion, Birkhäuser, Basel, 1997, p. 7.
[26] S.H. Zigmond, Recent quantitative studies of actin filament turnover during cell locomotion, Cell Motil. Cytoskeleton 25 (1993) 309.